

In situ borneol-modified polyester with antibacterial adhesion and long-term fungal-repellent properties

Zixu Xie^a, Chen Chen^a, Xinyu Chen^a, Fanqiang Bu^a, Guofeng Li^a, Pengfei Zhang^{a,b,*}, Xing Wang^{a,*}

^a Beijing Laboratory of Biomedical Materials, College of Life Science and Technology, Beijing University of Chemical Technology, Beijing 100029, China

^b Shanxi Province Key Laboratory of Oral Diseases Prevention and New Materials, School and Hospital of Stomatology, Shanxi Medical University, Taiyuan 030001, Shanxi, China

ARTICLE INFO

Keywords:

Borneol
Polyester
Antibacterial
Fungal repelling
Stereochemistry

ABSTRACT

Polyester is widely used in biomedical, textile, and food packaging fields. Therefore, enhancing it with antimicrobial properties would be a significant advancement. In this paper, a series of borneol-triazine polyesters (BTPs) with different structures are synthesized through room temperature polycondensation. The structure and composition of BTPs are systematically characterized by ¹H NMR, FTIR and GPC. Antimicrobial results reveal that the ability of BTPs to resist bacterial or fungal adhesion is directly related to the polymer structure. When the polymer chain of BTPs adopts a rigid structure, they exhibit excellent anti-adhesive and inhibitory performances against both Gram-negative bacteria (*Escherichia coli*) and Gram-positive bacteria (*Staphylococcus aureus*). Meanwhile, the as-synthesized BTPs poses a fungal-repelling effect on common fungal strains (*Aspergillus niger*) for up to 30 d. Further studies have shown that a stereochemical structure brought by borneol is key for imparting effective antimicrobial properties to BTPs. In addition, BTPs are non-leaching materials with low cellular cytotoxicity. Taking into consideration, BTP provides a potential strategy for preparing a new class of antimicrobial polyester materials.

1. Introduction

Polyester finds extensive application in sectors such as food packaging, medical devices, and textiles, ranking among the foremost polymer materials globally in annual consumption [1]. However, as public awareness of human health grows, traditional polyesters no longer meet the stringent antibacterial characteristics required by these industries [2–5]. Therefore, there arises a pressing necessity for antimicrobial advancements in polyester materials to address the challenges posed by the growth and spread of harmful microorganisms. Traditional approaches for producing antimicrobial polyesters include chemical post-modification of antibacterial components and physical mixing [6,7]. Unfortunately, polyesters often lack active functional groups, rendering subsequent chemical post-modification challenging [4]. Furthermore, while polyesters can acquire commendable bactericidal properties through physically blending with antimicrobial ingredients such as nanoparticles [8–10], cationic compounds [11] and antibiotics [12]. A significant challenge remains: these polyesters lose their bactericidal

effectiveness upon the ultimate release of the antimicrobial agents [13–16]. To overcome these difficulties, in situ modifying the structure of polyesters to impart intrinsic antibacterial characteristics is an appealing option [17].

A stereochemical antimicrobial adhesion technique has recently garnered considerable attention due to its enhanced antibacterial performance [18–20]. This antimicrobial method produces microbial adhesion resistance by selectively recognizing microorganisms' "chiral taste" of the material surface [21]. Numerous studies have shown that polymers containing chiral terpene monomers as antimicrobial components, when endowed with intrinsic antimicrobial adhesion properties in situ, exhibit good resistance to bacterial adhesion and fungal tropism [22–29]. Furthermore, our previous work has illustrated that menthol-triazine polyesters (MTPs) prepared by ambient polymerization possess the ability to resist microbial adhesion due to the influence of the antimicrobial component of menthol on the monocyclic monoterpene structure [30–32]. However, their antimicrobial adhesion effect remains inadequate, especially concerning their long-term ability to prevent

* Corresponding authors at: Beijing Laboratory of Biomedical Materials, College of Life Science and Technology, Beijing University of Chemical Technology, Beijing 100029, China.

E-mail addresses: pfzhang@sxmu.edu.cn (P. Zhang), wangxing@mail.buct.edu.cn (X. Wang).

<https://doi.org/10.1016/j.reactfunctpolym.2024.105993>

Received 19 February 2024; Received in revised form 13 June 2024; Accepted 21 June 2024

Available online 22 June 2024

1381-5148/© 2024 Elsevier B.V. All rights reserved, including those for text and data mining, AI training, and similar technologies.

bacterial growth and repel fungi. To develop a polyester with better antimicrobial adhesion, particularly long-term qualities, we chose L-borneol, a bicyclic monoterpene structure, as the antimicrobial component to manufacture the triazine-based polyester. However, under the same reaction conditions as menthol-based polymers, borneol does not react with triazine [33]. This is likely due to the greater steric hindrance of bicyclic monoterpene borneol compared to monocyclic monoterpene menthol. Therefore, it is necessary to explore suitable conditions to enhance the reactivity between borneol and triazine.

In this study, to achieve in situ antimicrobial modification of polyesters, a variety of borneol-triazine polyesters (BTPs) with diverse structures were synthesized by employing L-borneol as the antimicrobial component. Antibacterial adhesion assays and fungal repelling assays were used to study the anti-adhesive effect of different BTP structures on *Escherichia coli* (*E. coli*) and *Staphylococcus aureus* (*S. aureus*), as well as the fungal repellent effect on *Aspergillus niger* (*A. niger*). Furthermore, the mechanism of antimicrobial adhesion of BTPs was validated using the microbicide test, ZOI test, and contact angle (CA) test. Finally, the MTT assay was used to assess the cytotoxicity of BTPs. Overall, the prepared BTP series is projected to be a superior antimicrobial adhesion polyester, particularly with regard to long-term fungal repellence.

2. Experimental sections

2.1. Materials

L-Borneol, 2,4,6-triethylpyridine, terephthalic acid (TA), 1,3,5-triazine (TCT), 4-aminobenzoic acid (PABA), pyridine, diisopropylcarbodiimide (DIC), and ethanolamine were purchased from Aladdin Co. Malt extract agar, tryptic soy agar (TSA) and tryptic soy broth (TSB) were purchased from Beijing Auberger Co. The catalyst (4-(dimethylamino)pyridine-4-toluenesulfonate (DPTS)) for polyester synthesis was prepared according to the previously reported method [33]. All drugs were analytically pure. All solvents were purchased from Tianjin Damao Chemical Reagent Factory. The microbial strains used were obtained from the Chinese Industrial Culture Strain Bank. The strain types can be found in our previous work. The L929 cells used for cytotoxicity testing were obtained from the IBMS Cell Resource Center at CAMS/PIMC.

2.2. Preparation of borneol-derived monomers

2.2.1. Preparation of 2-borneol-4,6-chloro-1,3,5-triazine (TB)

9.36 g of L-borneol (0.06 mmol) was added to 20 mL of dichloromethane (DCM) and stirred until fully dissolved. Under an ice-water bath, 5.53 g of 1,3,5-triazine (0.03 mmol) and 4 g of 2,4,6-trimethylpyridine (0.04 mmol) were slowly added. The reaction proceeded for an additional 24 h. Subsequently, the mixed solution was subjected to three washes with saturated sodium chloride solution, and the organic phase was filtered. The product was purified using silica gel column chromatography (eluent was petroleum ether/DCM = 10:1) to give a white solid in about 85% yield. $^1\text{H NMR}$ (400 MHz, $\text{DMSO-}d_6$) δ 5.01 (s, 2H), 2.32 (s, 1H), 1.98 (s, 1H), 1.70 (s, 2H), 1.31 (s, 2H), 1.23 (s, 1H), 0.90 (s, 3H), 0.84 (s, 7H). $^{13}\text{C NMR}$ (151 MHz, DMSO) δ 160.40, 154.60, 150.62, 86.24, 49.27, 47.94, 44.56, 36.33, 27.84, 27.26, 19.88, 19.06, 13.70.

2.2.2. Synthesis of 2-borneol-4,6-ethanolamine-1,3,5-triazine (TBE)

1.81 g of DCMT (0.006 mol) was dissolved into 10 mL of DMF solution. Then 3.66 g of ethanolamine (0.06 mol) was added dropwise over half an hour. Then the temperature was increased to 100 °C, and the reaction proceeded for 24 h. Following cooling to room temperature, the mixed solution was washed with five volumes of deionized water, and the organic phase was separated. After solvent evaporation, the final white powder is obtained. The white powder was collected as a product, yielding approximately 89%. $^1\text{H NMR}$ (400 MHz, $\text{DMSO-}d_6$) δ 5.01 (s, 2H), 2.32 (s, 1H), 1.98 (s, 1H), 1.70 (s, 2H), 1.31 (s, 2H), 1.23 (s, 1H), 0.90 (s, 3H), 0.84 (s, 7H).

2.2.3. Synthesis of 2-borneol-4,6-triazine-1,3,5-benzoic acid (TBP)

1.82 g of DCMT (0.006 mol) was dissolved in 10 mL of DMF solution. At room temperature, 4.11 g of PABA (0.06 mol) and 0.23 g of pyridine were added dropwise. Then the temperature was then raised to 150 °C and reacted for 36 h. Upon cooling to room temperature, the mixture is poured into three times the volume of deionized water. After that, the mixed solution was acidified to pH = 3 with a dilute hydrochloric acid solution (1 mol/L), and the light-yellow powder was obtained through suction, filtration, and vacuum drying, yielding approximately 78%. $^1\text{H NMR}$ (400 MHz, $\text{DMSO-}d_6$) δ 5.01 (s, 2H), 2.32 (s, 1H), 1.98 (s, 1H), 1.70 (s, 2H), 1.31 (s, 2H), 1.23 (s, 1H), 0.90 (s, 3H), 0.84 (s, 7H).

2.3. Preparation of BTPs

The process of PBSA preparation is illustrated as a typical example of BTPs. 0.5 g DEBT (2 mmol), 0.24 g SA (2 mmol), 0.003 g DPTS (0.5 mol) and 2 mL of super-dry DCM were placed in a N_2 -filled reaction vial. Then 1.5 mL of DIC was added dropwise to the reaction system, and stirring was continued for about 1.5 h under an ice water bath. The reaction was then continued at room temperature for 24 h. Afterward, the crude product was dissolved in a small amount of DCM solution and precipitated in a large amount of cold methanol, repeating this process thrice. The precipitated product was collected and dried, yielding approximately 88%. $^1\text{H NMR}$ (400 MHz, $\text{DMSO-}d_6$) δ 7.30 (s, 1H), 4.09 (s, 3H), 3.44 (s, 3H), 3.17 (s, 1H), 2.53 (s, 3H), 1.98 (s, 1H), 1.62 (s, 1H), 1.25 (s, 1H), 1.16 (s, 1H), 0.88 (s, 3H), 0.81 (s, 3H).

PBET (yield of 85%. $^1\text{H NMR}$ (400 MHz, $\text{DMSO-}d_6$) δ 7.98 (s, 2H), 4.35 (s, 2H), 3.60 (s, 2H), 0.82 (s, 2H), 0.71 (s, 1H).)

PEBT (77% yield. $^1\text{H NMR}$ (400 MHz, $\text{DMSO-}d_6$) δ 10.09, 7.90, 4.90, 4.58, 2.13, 1.91, 1.61, 1.44, 1.27, 1.01, 0.84, 0.69.)

PBETB (71% yield. $^1\text{H NMR}$ (400 MHz, $\text{DMSO-}d_6$) δ 10.09 (s, 1H), 7.89 (s, 4H), 7.44 (s, 0H), 5.09 (s, 1H), 4.90 (s, 1H), 4.31 (s, 2H), 3.60 (s, 2H), 2.43 (s, 1H), 2.02 (s, 0H), 1.68 (s, 1H), 0.86 (s, 5H), 0.79 (s, 0H).)

2.4. Testing and characterization

$^1\text{H NMR}$ spectra of monomers and polyesters were tested on a Bruker AV-500 spectrometer (deuterated dimethyl sulfoxide ($\text{DMSO-}d_6$), tetramethylsilane (TMS)). Fourier transforms infrared (FTIR) spectra were tested on a Nicolet Avatar-360. Gel permeation chromatography (GPC) was tested on an Agilent instrument (Model 1100), eluent: tetrahydrofuran. The universal calibration method was used for GPC measurements. The water contact angle of the polymer material was measured by a CA-XP150 measuring instrument. The polymers were pressed into discs with a diameter of 13 mm and a thickness of 0.75 mm for antimicrobial testing.

2.5. Antibacterial adhesion assays

2.5.1. Antibacterial spreading test

A “sandwich structure” was used to observe the inhibition of bacterial growth by the polymer [31]. A 2 μL suspension of pre-prepared *E. coli* or *S. aureus* (10^6 CFU/mL) was dropped on the top “TSA island”, and the incubation was then incubated at 37 °C. Changes in the plate were recorded every 24 h using a digital camera.

2.5.2. Plate counting experiment

To quantitatively assess bacteria adhesion to the polymer, the antimicrobial adhesion efficiency of the material was evaluated following methods outlined in previous literature [31]. Prior to conducting the experiments, the polymer sheets were thoroughly sterilized. Initially, the polymer sheets were immersed in 1 mL of bacterial suspension and placed in a shaker at 120 rpm for 24 h. Subsequently, the material was removed and gently rinsed three times with deionized water. The material was submerged in 2 mL of PBS solution and agitated vigorously to completely disperse the bacteria adhering to the material. Then 100 μL

of the diluted solution was applied to the TSA medium and incubated at 37 °C for 24 h. Additionally, after three washes, the material was placed in 10 mL of sterile LB broth and incubated at 37 °C with shaking. The change in OD of the solution at 600 nm was measured every three hours to generate the bacterial growth curve.

2.6. Fungal repelling evaluation

The antifungal behavior of the polymeric tablets was studied by fungal repelling assay according to the previously reported method [23]. First, 10 μ L of *A. niger* suspension was dropped into the center of the culture medium, and then the material was placed approximately 15 mm away from the center. Subsequently, the plates were incubated at 30 °C and photographed to record the experimental phenomena.

2.7. Bactericidal evaluation

The bactericidal effect of the BTPs was assessed following the standardized procedure outlined in AATCC 100. 30 μ L of bacterial suspension (10^7 CFU/mL) was placed between two sterilized BTPs sheets, forming a sandwich structure. The sandwiched structures were then incubated at 37 °C for 24 h while maintaining a moist environment. Subsequently, the sandwich structure was transferred to a centrifuge tube, and 2 mL of sterile saline was added. The samples were washed with sterile saline under vigorous agitation. Serial 10-fold dilutions of 0.1 mL of the eluate were made and then plated onto TSA plates. Following incubation at 37 °C for 12 h, and the number of CFU was counted manually to calculate the bactericidal efficiency.

2.8. Fungicide evaluation

A simple contact killing method was used to investigate whether the polymer was fungicidal. 30 μ L of *A. niger* suspension (10^8 CFU/mL) was dropped between two sterilized polymer sheets, forming a sandwich structure. The sandwich structure was incubated at 30 °C for 24 h. A moist environment was maintained throughout the incubation to prevent desiccation of the fungal suspension. Subsequently, the material was inverted in the medium using the “stamp” method and removed after 30 s (the position of the placed fabric was marked). The medium was incubated in an incubator at 30 °C for 7 d to observe the growth of *A. niger*. Additionally, SEM was used to observe the microscopic morphology of *A. niger* and the material after 24 h of contact.

2.9. Zone of inhibition (ZOI) evaluation

The ZOI test was employed to examine whether BTPs eradicate bacteria through the release of small molecules. Briefly, 0.1 mL of bacterial suspension (10^7 CFU/mL) was dropped onto TSA medium and evenly spread. The BTPs tablets were then placed in the center of the medium and incubated at 37 °C for 24 h. The experimental phenomena were recorded with a digital camera.

2.10. Cytotoxicity evaluation

The cytotoxicity of BTPs was assessed by MTT assay on L929 mouse fibroblasts. Briefly, 0.2 g of sterilized material was immersed in 2 mL of 1640 extract in the addition of 10% FBS, 100 units/mL penicillin and 100 μ g/mL streptomycin as a complete cell culture medium. The cells were then incubated in a 37 °C cell incubator. After 48 h of incubation, cell viability was determined by MTT colorimetric assay and calculated the relative growth rate (RGR) of the cells.

3. Results and discussion

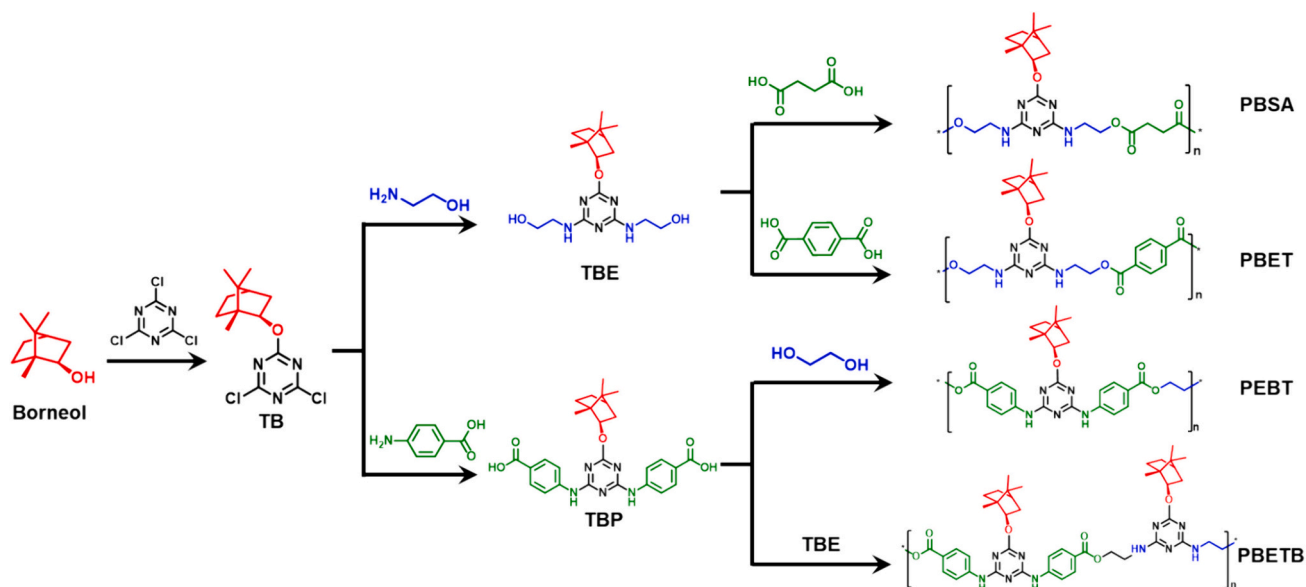
3.1. Synthesis and characterization of monomers

The preparation procedures of BTPs were showed in Scheme 1, and the chemical structures of three monomers (TB, TBE and TBP) were characterized by ^1H NMR. The protons of the hypomethyl group on the borneol appeared at 4.43 ppm. The protons of methyl and methylene species appeared in the range of 0.76 ppm–2.11 ppm, respectively. The alcoholic hydroxyl protons showed a signal at 3.78 ppm (Fig. S1A). Subsequent substitution reactions were carried out by the alcohol hydroxyl group of borneol and the chlorine atom of triazine. The substitution reaction of chlorine atoms on triazine is temperature-dependent. Monosubstitution can be carried out at 0 °C–10 °C, di-substitution requires 25 °C–40 °C, and tri-substitution requires 80 °C or even higher. However, no monosubstitution reaction between borneol and TCT occur under 0 °C–10 °C. After increasing the temperature to 40 °C, TB products with high reaction efficiency and yield were obtained without disubstitution of the borneol. This may be due to the unique structure of borneol, where the higher spatial site resistance of the cage structure leads to the need for higher temperatures for the monosubstitution reaction with triazine. The proton signal at 3.78 ppm disappeared due to the occurrence of triazine monosubstitution reaction. Since the triazine monomer did not have any proton, no new proton signal was generated in the ^1H NMR spectrum of TB (Fig. S1B). Therefore, borneol and TB was characterized through ^{13}C NMR (Fig. S1C and D). The carbon atom signal at position a of borneol shifted from 75.27 ppm to 86.24 ppm. Additionally, in Fig. S1D, three carbon atom peaks appeared at 150.62, 154.60, and 160.40 ppm, which correspond to the carbon atoms on the TCT ring, thus confirming the successful synthesis of TB. To design monomers suitable for polyester, the two chlorine atoms of the triazine group on TB were subsequently substituted with the amino groups of ethanolamine and p-aminobenzoic acid, respectively. Compared with the ^1H NMR spectrum of TB, the imino protons of TBE appeared at 6.96 and 6.84 ppm, the hydroxyl protons at 6.64 ppm, and the proton signals of methyl at 3.27 and 3.46 ppm, respectively (Fig. S1E). Compared with the ^1H NMR spectrum of TB, the carboxylate and imino protons of TBP appeared at 12.68 and 10.10 ppm, respectively, and the proton of benzene ring appeared at 7.90 ppm (Fig. S1F). Thus, TB, TBE and TBP were successfully synthesized.

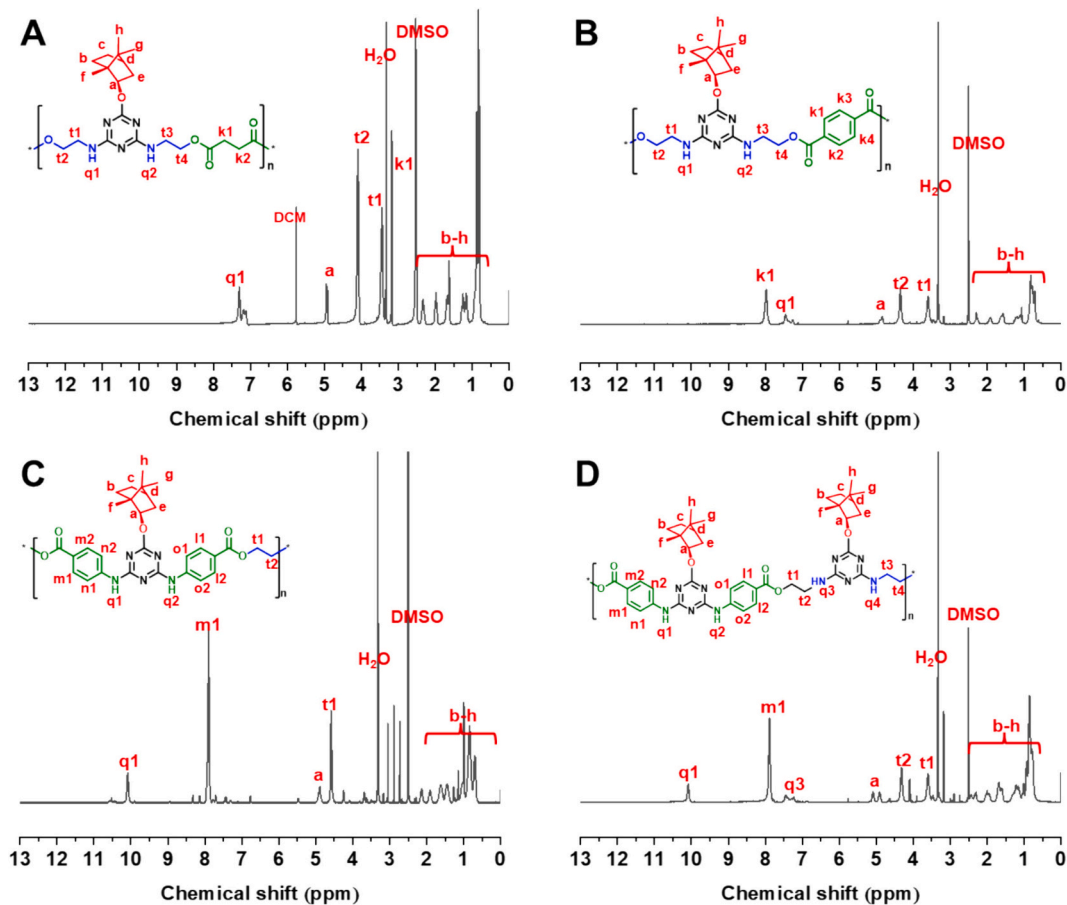
3.2. Synthesis and characterization of BTPs

The structure analysis of the BTPs was initially explored using FTIR (Fig. S2). Since the four polymers had similar structures, their FTIR spectra exhibited similar absorption peaks. All four BTPs showed stretching absorption of N–H at 3350 cm^{-1} and stretching absorption of $-\text{CH}_2$ at 2860 cm^{-1} . Since all BTPs had TCT structures, an absorption band characteristic of the C=N group stretching vibration appeared at 1500 cm^{-1} . The absorption peak observed at 1020 cm^{-1} was assigned to the C–O stretch of the ether group. Notably, the strong absorption of the C=O stretching peak of the carbonyl group at 1720 cm^{-1} indicated the presence of the ester. In addition, PBET, PEBT, and PBETB showed a characteristic absorption band for C=C aromatic vibrations around 1260 cm^{-1} due to the presence of the benzene ring in their structures. Conversely, PBSA lacked this absorption band owing to the absence of a benzene ring in its structure.

^1H NMR was used to further demonstrate the chemical structure of the BTPs. Firstly, all four BTPs showed characteristic absorption peaks representing borneol. The protons of the hypomethyl group of the borneol appeared at 4.43 ppm. The protons of methyl and methylene species appeared in the range of 0.76 ppm–2.11 ppm, respectively. For PBSA (Fig. 1A), the imino protons appeared at 6.96 and 6.84 ppm, respectively, and the methyl proton signals appeared at 3.46 and 4.12 ppm, respectively. The proton signal representing the methyl group on the chain link of succinic acid appeared at 3.27 ppm, respectively. In



Scheme 1. Procedures of preparation of BTBs (PBSA, PBET, PEPT and PBETB).

Fig. 1. ^1H NMR spectrum of (A) PBSA, (B) PBET, (C) PEPT and (D) PBETB.

addition, the proton signal of the carboxylic acid of succinic acid and the proton signal of the hydroxyl group of TBE at 6.64 ppm also disappeared. For PBET (Fig. 1B), the proton signal representing the benzene ring on the terephthalic acid linkage appeared at 8.10 ppm. In addition, no terephthalic acid carboxylic acid proton signal and TBE hydroxyl proton signal were found. For PEPT (Fig. 1C), the imino proton

appeared at 10.10 ppm and the proton of the benzene ring appeared at 7.90 ppm. The methyl proton signal representing the *p*-ethylene glycol linkage appeared at 4.62 ppm. In addition, no carboxylic acid proton signal or glycol hydroxyl proton signal was found for TBP. For PBETB (Fig. 1D), imino protons appeared at 6.96 and 6.84 ppm, methyl protons at 3.46 and 4.12 ppm, and benzene ring protons at 7.90 ppm. In

addition, no carboxylic acid proton signal of TBP and no hydroxyl proton signal of TBE were found. In conclusion, the FTIR and ^1H NMR results fully confirm the successful synthesis of BTPs. Borneol possesses larger steric hindrance compared to menthol, so the reaction between borneol and triazine cannot occur under the same conditions as menthol-based polymers. This study improves the efficiency of the reaction between borneol and triazine through modified methods, yielding approximately 85%.

The molecular weights of BTPs were also characterized by GPC. The results showed that the molecular weights of all four polymers were relatively large, ranging from 11,999–14,879 g/mol (Table. S1). In addition, the PDI of the molecular weights of these four polymers ranged from 1.28 to 1.66, indicating a narrow range of molecular weight distribution of BTPs.

3.3. Antibacterial adhesion evaluation

The performance of BTPs in inhibiting the growth of common bacterial species (*E. coli* and *S. aureus*) was first studied visually using a bacterial spreading model (Fig. 2A). Compared with PET, all four BTPs demonstrated different degrees of inhibition against the growth of both *E. coli* and *S. aureus* growth. As PET lacks antibacterial properties, the *E. coli* in the PET group could observe the appearance of rings on the medium around the material after 24 h of incubation. Furthermore, the radius of these rings progressively expanded with prolonged incubation time (Fig. 2B). For the PBSA group, the appearance of rings was not observed during the first 48 h of incubation. In comparison, rings began to appear around the material after 72 h of incubation, indicating that *E. coli* had broken through the limit of PBSA material by this time. Conversely, the other three groups of BTPs (PBET, PEET and PBEBT) showed no appearance of *E. coli* rings around them throughout the 120-h incubation period, indicating that *E. coli* could not break through the limit of these materials and grow further on the medium. A similar phenomenon was observed in the culture of *S. aureus*. Due to the strain difference with *E. coli*, the *S. aureus* in the PET group showed a yellow ring around the material after 48 h incubation. The radius progressively

increased with extended incubation time (Fig. 2C). PBSA showed a few rings around the material only after 72 h of incubation, which indicated that PBSA inhibited the growth of *S. aureus* to some extent. The other three groups of BTPs (PBET, PEET and PBEBT) showed no appearance of *S. aureus* rings around them throughout the incubation of 120 h, indicating that *S. aureus* could not break through the material and grow further on the medium. Although PBSA demonstrated some degree of efficacy in inhibiting the growth of two bacteria, it remained less competitive than the other three polymers, which consistent with our previous findings [32]. The main chain structure of PBSA is more flexible than the other three BTPs, which may cause the wrapping of the polymer chains around the borneol moiety, thus causing a deficiency in the amount of borneol moiety exposure and thus significantly reducing the bacterial growth inhibition of PBSA. In addition, the results of PBET, PEET and PBEBT showed that these three BTPs could effectively inhibit bacterial growth within 120 h.

Next, the antimicrobial adhesion efficiency of the four BTPs against *E. coli* and *S. aureus* was evaluated using the bacterial colony counting method. Given that most bacterial infections originate from the initial adhesion of bacteria to the material surface, inhibiting this initial attachment of bacteria is pivotal in infection prevention. After 24 h of contact with the bacterial suspension, the bacteria easily adhered to the surface of the PET material, as PET inherently lacks antimicrobial activity (Fig. 3A). Specifically, the statistical analysis revealed approximately 7.74×10^3 CFU of *E. coli* and 9.25×10^3 CFU of *S. aureus* adhering to the PET surface. In comparison to PET, the number of bacteria adhering to the surface of the four BTPs showed a different degree of reduction. The number of *E. coli* and *S. aureus* adhering to the surface of PBSA was about 1.81×10^3 CFU and 2.5×10^3 CFU (Fig. 3B and C). The resistance efficiency against both bacterial adhesions remained above 70%. The number of *E. coli* and *S. aureus* adhering to the surface of PBET and PEET was maintained at 300–400 CFU, resulting in a resistance efficiency of over 90%. Conversely, adhesion of *E. coli* and *S. aureus* was nearly imperceptible on the surface of PBETB, with only 20 CFU adhering. PBETB exhibited the highest efficiency of anti-adhesion of both bacteria, surpassing a remarkable 99.7% efficiency

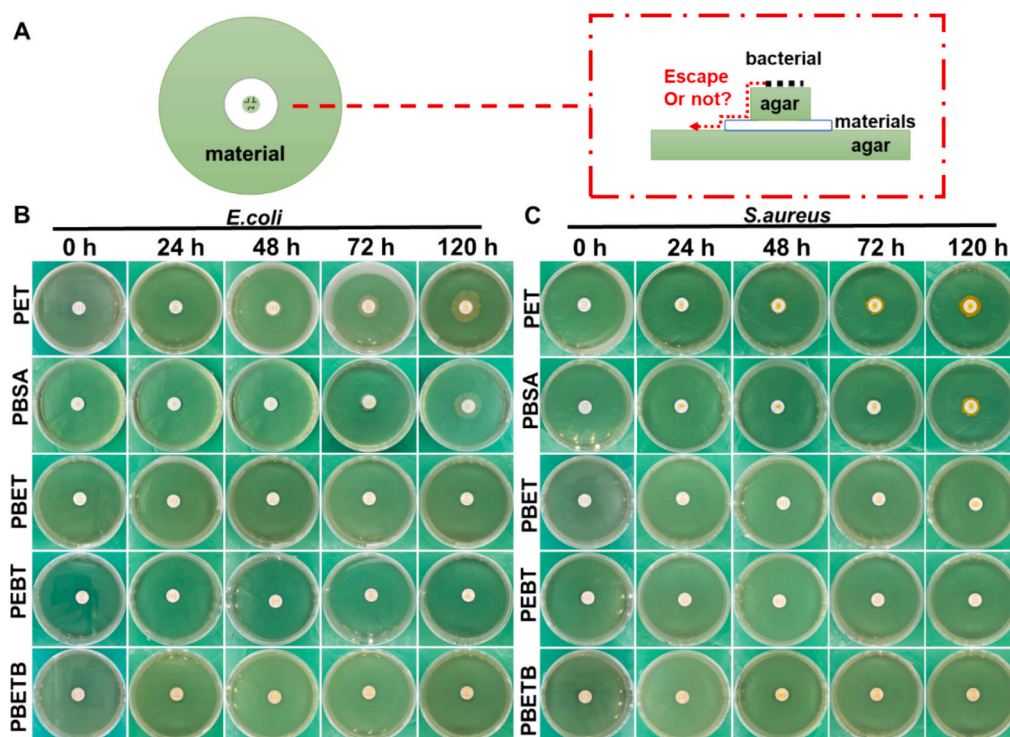


Fig. 2. (A) Schematic diagram of antibacterial spreading test. Photographs of agar plates of polymer against (B) *E. coli* and (C) *S. aureus* for 120 h.

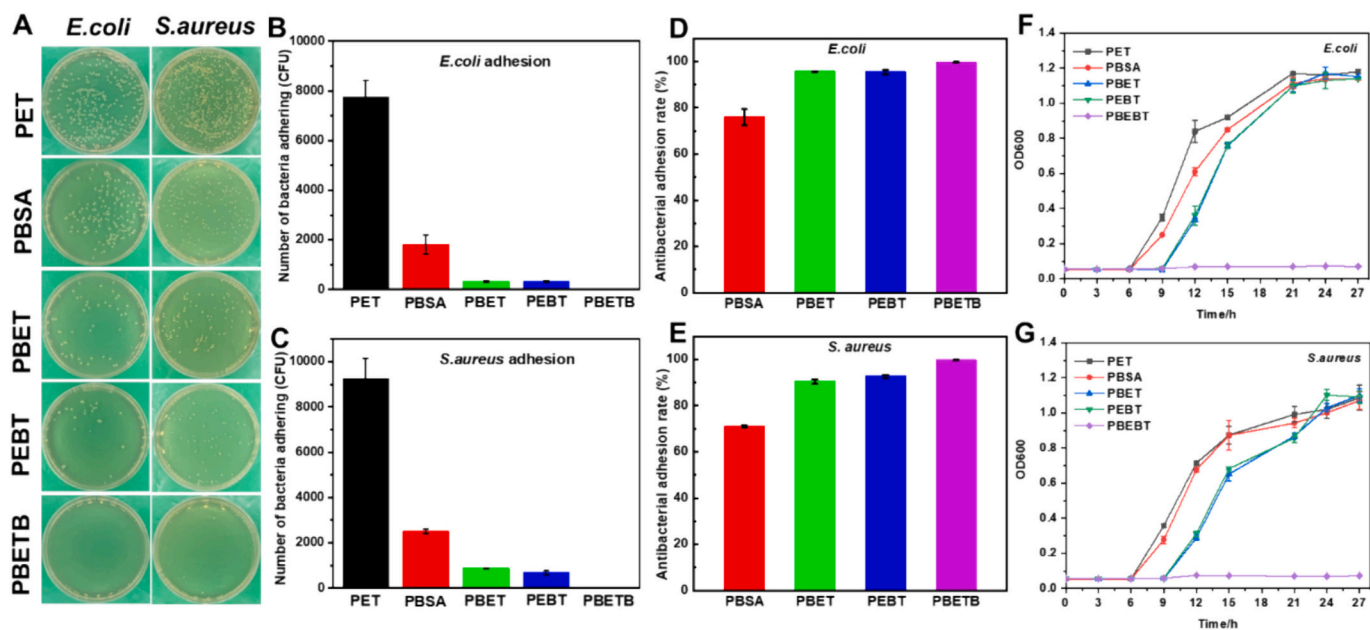


Fig. 3. A quantitative study of antibacterial adhesion. (A) Photographs of agar plates of polymer against *E. coli* & *S. aureus*; (B) The number of bacteria adhering to the polymers against *E. coli*; (C) The number of bacteria adhering to the polymers against *S. aureus*; (D) Antibacterial adhesion rate of the polymers against *E. coli*; (E) Antibacterial adhesion rate of the polymers against *S. aureus*. (F) Optical density 600 test results to evaluate the antibacterial properties of the polymer against *E. coli*; (G) Optical density 600 test results to evaluate the antibacterial properties of the polymer against *S. aureus*.

(Fig. 3D and E). The pattern of quantitative plate count assessments was also consistent with the results obtained from the bacterial spreading experiment. Then OD experiments were also employed to validate this variation pattern. The difference in the number of initial colonies was reflected in the change in OD of *E. coli* (Fig. 3F) and *S. aureus* (Fig. 3G) attached to the material surface. After 6 h of incubation, the *E. coli* in the PET and PBSA groups had just transitioned from the lag phase to the log phase of bacterial growth. In contrast, the log phase of bacterial growth in the PBET and PEPT groups appeared only after 9 h. In contrast, the PBETB never showed the log phase of bacterial growth. After 12 h of incubation, the corresponding OD values exhibited a clear gradient of bacterial density, ranging from low to high, in the sequence of PBETB, PBET, PEPT, PBSA and PET, revealing differences in the effectiveness of

various BTP structures against *E. coli* adhesion. For *S. aureus*, a similar pattern of OD changes can be observed. Thus, all four BTPs showed different degrees of resistance to *E. coli* and *S. aureus* adhesion, and the antibacterial adhesion effect was closely related to the structural differences of the BTPs.

3.4. Antifungal adhesion evaluation

The resistance of BTPs to fungal contamination was evaluated by visualizing an experimental model of fungal repulsion. *A. niger* was selected as the experimental strain for this model, and the cultivation period extended to 30 d. *A. niger* typically spreads in a circular pattern from the center towards the periphery of the medium. When it touches

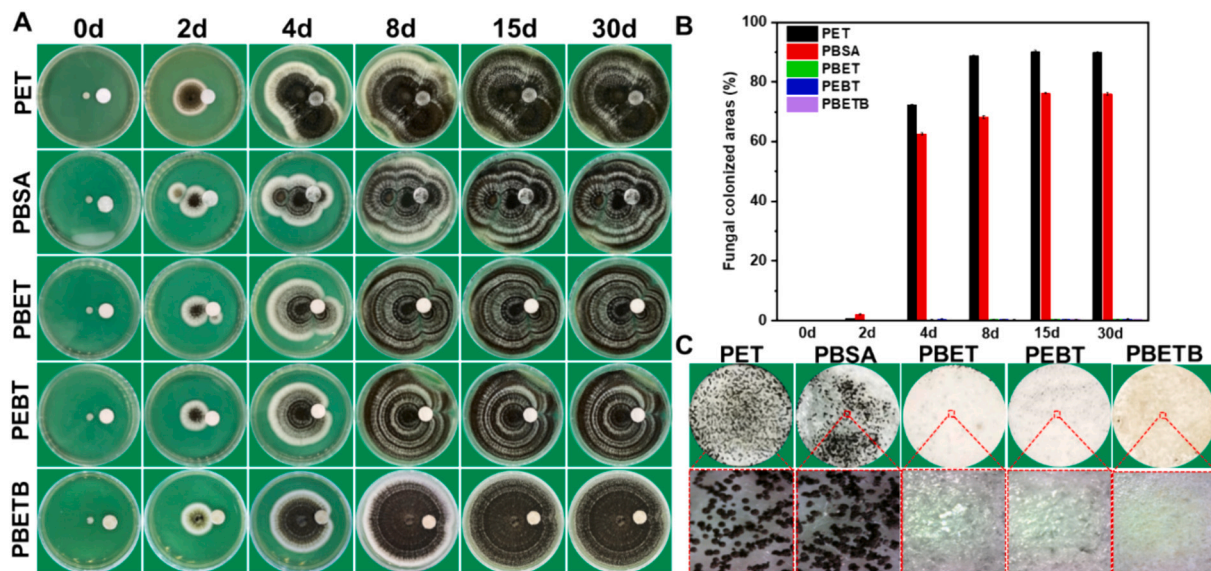


Fig. 4. The fungal repelling evaluation. (A) Photographs of the growth of *A. niger* in the PET and PEPT groups within 72 h. (B) Fungal colonized areas (%) after 0, 2, 4, 8, 15, and 30 d of incubation. (C) The magnified image is micrographs of polymers' surfaces at 30 d.

the edge of the material, it possesses the option to climb up or continue to grow around the material, thus determining whether the material can resist fungal contamination. After 2 d of incubation, the mycelium of *A. niger* started to touch the edges of the material (Fig. 4A), resulting in the emergence of a small quantity of *A. niger* on the surface of PET and PBSA, with a colonization area of about 1.2% and 2.1% (Fig. 4B). In contrast, the surfaces of PBET, PEBT and PBETB were temporarily free of *A. niger*. After 4 d of incubation, the surface of PET and PBSA was rapidly covered with the large number of *A. niger* visible to the naked eye, with the percentage of the colonized area reaching 72.3% and 62.6% respectively. In stark contrast, the percentage of *A. niger* colonization on the surfaces of PBET, PEBT, and PBETB was merely 0.3–0.4%, rendering it nearly negligible. During the subsequent 30 d incubation, the coverage rate of *A. niger* on the surface of PET and PBSA materials slowed down significantly, and the percentage of the colonized area was stabilized at 89.9% and 76.0%. In contrast, *A. niger* was barely visible on the surfaces of PBET, PEBT, and PBETB, with the colonization area maintained at about 0.5%. The microscopic images of the material surfaces also showed this pattern (Fig. 4C). Black spores were visible on the surfaces of PET and PBSA. In contrast, the surfaces of PBET, PEBT, and PBETB were completely clean without any spores being detected. Consequently, the ability of PBSA to resist *A. niger* adhesion is limited, while PBET, PEBT, and PBETB demonstrate effective resistance against *A. niger* contamination for up to 30 days.

3.5. Antimicrobial mechanism

In our previous reports, MTPs achieved anti-adhesive effects against bacteria and fungi through a chiral antimicrobial adhesion strategy rather than through microbicidal effects [30]. Therefore, it is worthwhile to investigate whether the outstanding antimicrobial properties observed in BTPs are also attained through this strategy. To assess this, we employed the contact sterilization method to evaluate the bactericidal or fungicidal properties of BTPs. After 24 h of contact between the four BTPs and the bacterial suspensions, the bacterial suspensions was

then subjected to plate coating experiment. The results of plate coating experiment revealed that the four BTPs did not show any significant reduction in colony number compared to the PET group for either *E. coli* or *S. aureus* (Fig. 5A). In addition, upon analyzing the colony counts, it can be seen that the colony counts of *E. coli* remained between 4×10^5 – 4.5×10^5 CFU in the PET group and the four BTPs groups, with no significant differences observed among them (Fig. 5B). Similarly, and the colony counts of *S. aureus* remained between 6×10^5 – 6.5×10^5 CFU (Fig. 5C). This indicates that all four types of BTPs are unable to kill *E. coli* and *S. aureus*. On the other hand, in the fungicidal test, it is observed that *A. niger* spores maintain normal growth and reproduction even after 24 h of contact with the material. Meanwhile, the growth of *A. niger* in the PET group and the four BTPs groups were similar (Fig. 5D). The microscopic images of *A. niger* and the material after 24 h contact showed that the microscopic surface of it in the BTPs groups were still complete without signs of shrinkage or rupture compared with the PET group (Fig. S3). Therefore, the four BTPs were unable to kill *A. niger*. Further, the ZOI test was conducted to confirm whether small molecules were released from the BTPs. The results showed that none of the four BTPs showed inhibition zones around them, confirming that the BTPs are non-leaching polymers. In addition, the adhesion behavior of microorganisms is influenced by the wettability of the material. Therefore, the water contact angles of the BTPs were measured (Fig. 5F). The results showed that the CA of the BTPs increased and behaved more hydrophobic with the introduction of the borneol moiety, which was attributed to the hydrophobic cage-like structure of the borneol. Among the four BTPs, PBETB exhibited the highest hydrophobicity. An increase in the density of the introduced hydrophobic groups results in a corresponding increase in the hydrophobicity of the BTPs. Importantly, it has been reported that the effect of hydrophobicity of the material on the antimicrobial adhesion properties is not simply a positive correlation [21]. Additionally, the adhesion of bacteria and fungi on stereochemical modified materials was not related to hydrophobicity [22]. Taken together, the borneol moiety with a unique stereochemical structure in BTPs plays a crucial role in antimicrobial adhesion.

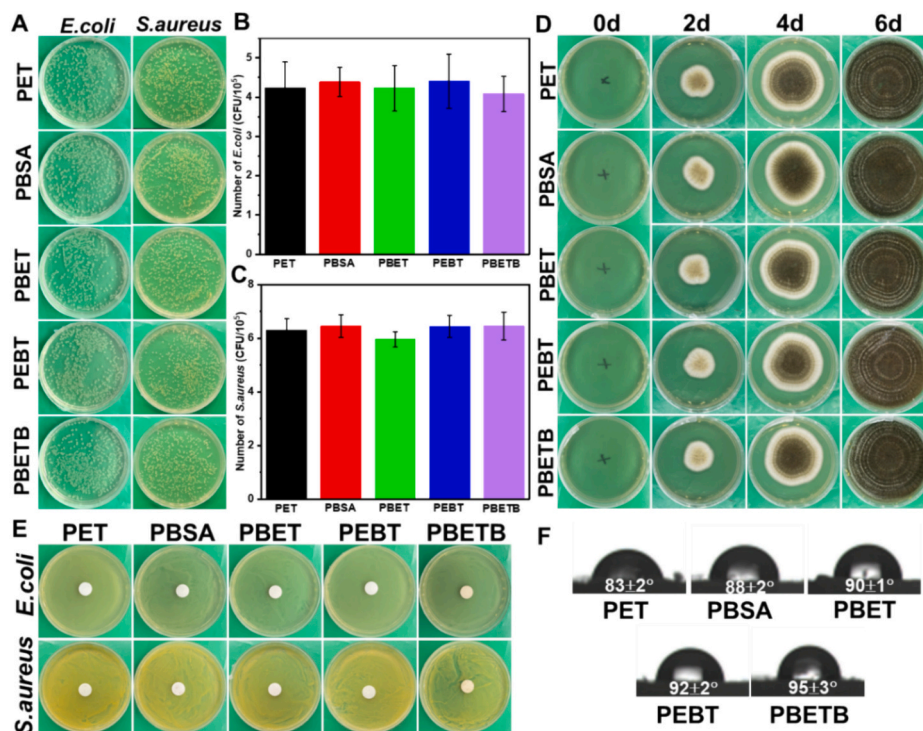


Fig. 5. Study of antimicrobial mechanisms. (A) Photographs of agar plates of polymer against *E. coli* & *S. aureus*; (B) The number of bacteria of the polymers against *E. coli*. (C) The number of bacteria in the polymers against *S. aureus*. (D) Results of fungicide experiment. (E) ZOI Test of the polymers against *E. coli* and *S. aureus*. (F) CA of polymers.

3.6. Cytotoxicity evaluation

The cytotoxicity of BTPs was also evaluated by MTT assay. The relative growth rates (RGR) of L929 cells and PET and BTPs were all maintained above 90% after co-incubation for 48 h (Fig. S4). The cytotoxicity of all these polyesters was grade 1 according to the standard toxicity class (ISO 10993-5: 2009) (Table S1). Therefore, BTPs are a class of antimicrobial material without cytotoxicity.

4. Conclusion

In summary, this study developed an modified method to enable the substitution reaction between borneol and triazine. Then, three borneol-triazine monomers and a range of borneol-triazine polyesters (BTPs) were developed via room temperature polyesterizing with succinic acid, terephthalic acid or ethylene glycol. Results showed that the antimicrobial adhesion properties of BTPs were closely related to their structures. BTPs with a rigid chain structure demonstrated more than 95% anti-adhesion effectiveness against bacteria (*E. coli* and *S. aureus*) and a prolonged *A. niger* repellent effect lasting more than 30 days. Further studies revealed that BTPs cannot kill bacteria or fungi, and its antimicrobial adhesion properties are derived from the borneol, which has a stereochemical structure. Furthermore, BTPs were a non-leaching polyester class with minimal cytotoxicity. We are confident that this research contributes to a better understanding of stereochemistry in the in situ antimicrobial modification of polyesters and sets the groundwork for future applications of stereochemical techniques in the structural design of antimicrobial polyesters.

CRedit authorship contribution statement

Zixu Xie: Writing – review & editing, Writing – original draft, Visualization, Software, Methodology, Investigation, Data curation. **Xinyu Chen:** Writing – review & editing. **Fanqiang Bu:** Writing – review & editing. **Guofeng Li:** Writing – review & editing, Data curation. **Pengfei Zhang:** Writing – review & editing, Methodology, Investigation, Formal analysis. **Xing Wang:** Supervision, Project administration, Funding acquisition, Conceptualization.

Declaration of competing interest

The authors declare that they have no known competing financial interests or personal relationships that could have appeared to influence the work reported in this paper.

Data availability

Data will be made available on request.

Acknowledgements

The authors thank the National Natural Science Foundation of China (52273118, 22275013) for their financial support. Additionally, thank Wensheng Xie for revision of the manuscript.

Appendix A. Supplementary data

Supplementary data to this article can be found online at <https://doi.org/10.1016/j.reactfunctpolym.2024.105993>.

References

- [1] J. Yan, L. Zheng, K. Hu, L. Li, C. Li, L. Zhu, H. Wang, Y. Xiao, S. Wu, J. Liu, B. Zhang, F. Zhang, Cationic polyesters with antibacterial properties: facile and controllable synthesis and antibacterial study, *Eur. Polym. J.* 110 (2019) 41–48, <https://doi.org/10.1016/j.eurpolymj.2018.11.009>.
- [2] A. Bashiri Rezaie, M. Montazer, M. Mahmoudi Rad, Low toxic antibacterial application with hydrophobic properties on polyester through facile and clean fabrication of nano copper with fatty acid, *Mater. Sci. Eng. C* 97 (2019) 177–187, <https://doi.org/10.1016/j.msec.2018.12.008>.
- [3] Z. Zhang, Y. Cao, J. Gu, J. Li, Y. Wang, S. Chen, Giant persistent antimicrobial and biocompatible polyester fabrics for anti-mold food packaging, *Mater. Today Chem.* 22 (2021) 100571, <https://doi.org/10.1016/j.mtchem.2021.100571>.
- [4] X. Ding, S. Duan, X. Ding, R. Liu, F.-J. Xu, Versatile antibacterial materials: an emerging arsenal for combatting bacterial pathogens, *Adv. Funct. Mater.* 28 (2018) 1802140, <https://doi.org/10.1002/adfm.201802140>.
- [5] W. Zhai, Y. Cao, Y. Li, M. Zheng, Z. Wang, MoO₃-x QDs/MXene (Ti3C₂Tx) self-assembled heterostructure for multifunctional application with antistatic, smoke suppression, and antibacterial on polyester fabric, *J. Mater. Sci.* 57 (2022) 2597–2609, <https://doi.org/10.1007/s10853-021-06690-8>.
- [6] H. Zhang, T. Fang, X. Yao, Y. Xiong, W. Zhu, Large scale production of catalyst-free poly(ethylene succinate) with intrinsic antibacterial property through the design of hyperthermostable quaternary ammonium monomers, *Chem. Eng. J.* 440 (2022) 135949, <https://doi.org/10.1016/j.cej.2022.135949>.
- [7] K. Wu, J. Li, X. Chen, J. Yao, Z. Shao, Synthesis of novel multi-hydroxyl N-halamine precursors based on barbituric acid and their applications in antibacterial poly(ethylene terephthalate) (PET) materials, *J. Mater. Chem. B* 8 (2020) 8695, <https://doi.org/10.1039/d0tb01497d>.
- [8] C. Shuai, Y. Xu, P. Feng, G. Wang, S. Xiong, S. Peng, Antibacterial polymer scaffold based on mesoporous bioactive glass loaded with in situ grown silver, *Chem. Eng. J.* 374 (2019) 304–315, <https://doi.org/10.1016/j.cej.2019.03.273>.
- [9] L. Mei, X. Zhang, Y. Wang, W. Zhang, Z. Lu, Y. Luo, Y. Zhao, C. Li, Multivalent polymer–Au nanocomposites with cationic surfaces displaying enhanced antimicrobial activity, *Polym. Chem.* 5 (2014) 3038–3044, <https://doi.org/10.1039/C3PY01578E>.
- [10] P. Zhang, J. Qi, R. Zhang, Y. Zhao, J. Yan, Y. Gong, X. Liu, B. Zhang, X. Wu, X. Wu, C. Zhang, B. Zhao, B. Li, Recent advances in composite hydrogels: synthesis, classification, and application in the treatment of bone defects, *Biomater. Sci.* 12 (2024) 308–329, <https://doi.org/10.1039/D3BM01795H>.
- [11] Y. Hu, Y. Wang, X. Zhang, J. Qian, X. Xing, X. Wang, Regenerated cationic dyeable polyester deriving from poly(ethylene terephthalate) waste, *Polym. Degrad. Stab.* 179 (2020) 109261, <https://doi.org/10.1016/j.polydegradstab.2020.109261>.
- [12] R. Scaffaro, L. Botta, A. Maio, G. Gallo, PLA graphene nanoplatelets nanocomposites: physical properties and release kinetics of an antimicrobial agent, *Compos. B Eng.* 109 (2017) 138–146, <https://doi.org/10.1016/j.compositesb.2016.10.058>.
- [13] R. Bai, J. Kang, O. Simalou, W. Liu, H. Ren, T. Gao, Y. Gao, W. Chen, A. Dong, R. Jia, Novel N-Br bond-containing N-Halamine nanofibers with antibacterial activities, *ACS Biomater. Sci. Eng.* 4 (2018) 2193–2202, <https://doi.org/10.1021/acsbiomaterials.7b00996>.
- [14] J.-Y. Huang, X. Li, W. Zhou, Safety assessment of nanocomposite for food packaging application, *Trends Food Sci. Technol.* 45 (2015) 187–199, <https://doi.org/10.1016/j.tifs.2015.07.002>.
- [15] Y. Zou, Y. Zhang, Q. Yu, H. Chen, Dual-function antibacterial surfaces to resist and kill bacteria: painting a picture with two brushes simultaneously, *J. Mater. Sci. Technol.* 70 (2021) 24–38, <https://doi.org/10.1016/j.jmst.2020.07.028>.
- [16] C. Zhang, Y. Li, Z. Li, Y. Jiang, J. Zhang, R. Zhao, J. Zou, Y. Wang, C. Ma, Q. Zhang, Nanofiber architecture engineering implemented by electrophoretic-induced self-assembly deposition technology for flash-type memristors, *ACS Appl. Mater. Interfaces* 14 (2022) 3111–3120, <https://doi.org/10.1021/acsaami.1c22094>.
- [17] L. Ding, L. Liu, Y.F. Chen, Y. Du, S.J. Guan, Y. Bai, Y. Huang, Modification of poly(ethylene terephthalate) by copolymerization of plant-derived A-truxillic acid with excellent ultraviolet shielding and mechanical properties, *Chem. Eng. J.* 374 (2019) 1317–1325, <https://doi.org/10.1016/j.cej.2019.05.224>.
- [18] L. Luo, G. Li, D. Luan, Q. Yuan, Y. Wei, X. Wang, Antibacterial adhesion of borneol-based polymer via surface chiral stereochemistry, *ACS Appl. Mater. Interfaces* 6 (2014) 19371–19377, <https://doi.org/10.1021/am505481q>.
- [19] J. Xu, Z. Xie, F. Du, X. Wang, One-step anti-superbug finishing of cotton textiles with dopamine-menthol, *J. Mater. Sci. Technol.* 69 (2021) 79–88, <https://doi.org/10.1016/j.jmst.2020.08.007>.
- [20] A.L. Hook, C.-Y. Chang, J. Yang, J. Luckett, A. Cockayne, S. Atkinson, Y. Mei, R. Bayston, D.J. Irvine, R. Langer, D.G. Anderson, P. Williams, M.C. Davies, M. R. Alexander, Combinatorial discovery of polymers resistant to bacterial attachment, *Nat. Biotechnol.* 30 (2012) 868–875, <https://doi.org/10.1038/nbt.2316>.
- [21] G. Li, H. Zhao, J. Hong, K. Quan, Q. Yuan, X. Wang, Antifungal graphene oxide-borneol composite, *Colloids Surf. B: Biointerfaces* 160 (2017) 220–227, <https://doi.org/10.1016/j.colsurfb.2017.09.023>.
- [22] J. Xu, Y. Bai, M. Wan, Y. Liu, L. Tao, X. Wang, Antifungal paper based on a polyborneolacrylate coating, *Polymers (Basel)* 10 (2018) 1–12, <https://doi.org/10.3390/polym10040448>.
- [23] C. Chen, Z. Xie, P. Zhang, Y. Liu, X. Wang, Cooperative enhancement of fungal repellence performance by surface photografting of stereochemical bi-molecules, *Colloids Interf. Sci. Commun.* 40 (2021) 100336, <https://doi.org/10.1016/j.colcom.2020.100336>.
- [24] L. Yang, C. Zhan, X. Huang, L. Hong, L. Fang, W. Wang, J. Su, Durable antibacterial cotton fabrics based on natural borneol-derived anti-MRSA agents, *Adv. Healthc. Mater.* 9 (2020) 2000186, <https://doi.org/10.1002/adhm.202000186>.
- [25] J. Hu, B. Sun, H. Zhang, A. Lu, H. Zhang, H. Zhang, Terpolymer resin containing bioinspired borneol and controlled release of camphor: synthesis and antifouling

- coating application, *Sci. Rep.* 10 (2020) 10375, <https://doi.org/10.1038/s41598-020-67073-8>.
- [26] F. Song, L. Zhang, R. Chen, Q. Liu, J. Liu, J. Yu, P. Liu, J. Duan, J. Wang, Bioinspired durable antibacterial and antifouling coatings based on borneol fluorinated polymers: demonstrating direct evidence of antiadhesion, *ACS Appl. Mater. Interfaces* 13 (2021) 33417–33426, <https://doi.org/10.1021/acscami.1c06030>.
- [27] X. Wang, S. Jing, Y. Liu, S. Liu, Y. Tan, Diblock copolymer containing bioinspired borneol and dopamine moieties: synthesis and antibacterial coating applications, *Polymer (Guildf)* 116 (2017) 314–323, <https://doi.org/10.1016/j.polymer.2017.03.078>.
- [28] X. Chen, Q. Nie, Y. Shao, Z. Wang, Z. Cai, TiO₂ nanoparticles functionalized borneol-based polymer films with enhanced photocatalytic and antibacterial performances, *Environ. Technol. Innov.* 21 (2021) 101304, <https://doi.org/10.1016/j.eti.2020.101304>.
- [29] J. Wu, C. Wang, C. Mu, W. Lin, A waterborne polyurethane coating functionalized by isobornyl with enhanced antibacterial adhesion and hydrophobic property, *Eur. Polym. J.* 108 (2018) 498–506, <https://doi.org/10.1016/j.eurpolymj.2018.09.034>.
- [30] J. Li, P. Zhang, M. Yang, Z. Xie, G. Li, X. Wang, Antimicrobial modification of PET by insertion of menthoxy-triazine, *ACS Appl. Polym. Mater.* 4 (2022) 1922–1930, <https://doi.org/10.1021/acscapm.1c01775>.
- [31] P. Zhang, J. Li, M. Yang, L. Huang, F. Bu, Z. Xie, G. Li, X. Wang, Inserting menthoxytriazine into poly(ethylene terephthalate) for inhibiting microbial adhesion, *ACS Biomater. Sci. Eng.* 8 (2022) 570–578, <https://doi.org/10.1021/acsbomaterials.1c01448>.
- [32] P. Zhang, M. Yang, J. Li, Z. Xie, G. Li, X. Wang, Menthoxytriazine modified poly(ethylene terephthalate) for constructing anti-adhesion surface, *Colloid Interf. Sci. Commun.* 46 (2022) 100567, <https://doi.org/10.1016/j.colcom.2021.100567>.
- [33] E.A. Chamsaz, S. Sun, M.V.S.N. Maddipatla, A. Joy, Photoresponsive polyesters by incorporation of alkoxyphenacyl or coumarin chromophores along the backbone, *Photochem. Photobiol. Sci.* 13 (2014) 412–421, <https://doi.org/10.1039/C3PP50311A>.